

Detection of microcalcifications in digital mammograms using the dual-tree complex wavelet transform

V. Alarcon-Aquino¹, O. Starostenko¹, J. M. Ramirez-Cortes², R. Rosas-Romero¹,
J. Rodriguez-Asomoza¹, O. J. Paz-Luna¹ and K. Vazquez-Muñoz¹

¹Communications and Signal Processing Research Group, Department of Computing, Electronics, and Mechatronics, Universidad de las Americas Puebla, Sta. Catarina Martir, Cholula, Puebla. 72820 Mexico. E-mail: vicente.alarcon@udlap.mx

²Department of Electronics Engineering, National Institute for Astrophysics, Optics, and Electronics, Tonantzintla, Puebla, Mexico

In this paper we propose an approach to detect microcalcifications in digital mammograms using the dual-tree complex wavelet transform (DT-CWT). The approach follows four basic strategies, namely, image denoising, band suppression, morphological transformation and inverse complex wavelet transform. Recently, the DT-CWT has shown a good performance in applications that involve image processing due to more data phase information, shift invariance, and directionality than other wavelet transforms. The procedure of image denoising is carried out with a thresholding algorithm that computes recursively the optimal threshold at each level of wavelet decomposition. In order to maximise the detection a morphological conversion is then proposed and applied to the high frequencies subbands of the wavelet transformation. This procedure is applied to a set of digital mammograms from the mammography image analysis society (MIAS) database. Experimental results show that the proposed denoising algorithm and morphological transformation in combination with the DT-CWT procedure performs better than the stationary and discrete wavelet transforms and the top-hat filtering. The approach reported in this paper seems to be meaningful to aid in the results on mammogram interpretation and to get an earlier and opportune diagnostic for breast cancer.

Keywords: Microcalcifications, dual-tree complex wavelet transforms, Mammography, breast cancer, MIAS database, wavelets.

1. INTRODUCTION

A mammography exam, called a mammogram, is used to aid in the diagnosis of breast diseases in women. A mammogram is a specialised X-ray exam in which a set of plates is taken from breast tissue to detect suspect tissue and microcalcifications (MCs). The main reason to perform a mammogram is the detection of clinically hidden breast cancer at early time. The early detection of breast cancer with a mammogram is difficult due to the fact that small tumours and MCs are very similar to normal glandular tissue. Recently, tools for computer-aided diagnosis have been developed especially in the image-

processing field that permits an easy visualisation of mammograms. In this regard, the wavelet transform (WT) has an important merit, since it has been employed to eliminate noise in mammogram image. The results have shown an improvement of the image, making easy the visualisation of suspicious lesions [1]. The WT analysis provides good time resolution and poor frequency resolution at high frequencies, and good frequency resolution and poor time resolution at low frequencies. Wavelets are a powerful tool to image compression with low information losses and have been applied in biomedical signals because they provide an analysis of non-stationary signals that contains a high amount of complex frequencies [1].

Lately, several approaches have been proposed to detect MCs in digital mammograms. A system based on fuzzy logic has been reported in [2], a mathematical morphologist study is reported in [3], and several methods based on wavelet transforms are reported in [4–8, 12, 14, 18, 21]. For example in [4] Strickland and Hahn introduced a two stages method for detection and segmentation of MCs. The first stage is based on the use of undecimated wavelet transform and the segmentation process is realised with matched filters. A similar approach is also reported in [18]. In [5], Wang and Karayiannis reported an approach to detect MCs using the decimated wavelet transform so that suppression in the low-band frequencies is performed. The visualisation of MCs is improved using a non-linear threshold based on the arc-tan method. In [6], Melloul and Joscowicz proposed MCs detection in two steps. The first consists in total elimination of background mammogram with multi-scale morphological filtering then an optimal threshold (entropy threshold) is applied to segmentation step. In [14] an algorithm for early breast cancer diagnosis that employs a combination of neural networks and wavelet-based subband image decomposition that detects microcalcifications in digital mammograms is proposed. This algorithm uses a wavelet transform that performs the wavelet decomposition through a down-sampling process, which produces shifting. In general, the aforementioned approaches have disadvantages that limit the performance of these methods in image processing applications. These disadvantages are shift sensibility derived from the down-sampling process of the discrete wavelet transform, low directionality of the horizontal, vertical and diagonal orientations of the image, and information inexistence about phase.

In this paper we report an approach to detect microcalcifications in digital mammograms using the dual-tree complex wavelet transform (DT-CWT). The DT-CWT has shown a good performance in applications that involve image processing due to more data phase information, shift invariance, and directionality than other wavelet transforms. The approach consists of four stages, namely, image denoising by optimal thresholding, band suppression of low frequencies, morphological transformation, and inverse complex wavelet transform. The remainder of this paper is organised as follows. In Section 2, a description of MCs and MIAS database is presented. Section 3 presents an overview of wavelet theory including the DT-CWT. The proposed approach to detect microcalcifications is reported in Section 4. Experimental results are reported in Section 5. Conclusions and future work are discussed in Section 6.

2. DESCRIPTION OF MCS IN MAMMOGRAMS

Initially, the breast tissue study was performed in the radiology field by analogical images including all kind of image modalities such as magnetic resonance image and nuclear medicine. The basic idea for using different image methods was to detect and to diagnose at early stage the breast cancer tissue when the probability of cure was greater and the treatment was less aggressive. It helped by some means to decide the best therapy for each lesion. Currently, mammogram screening is the

only way for detection at a short period of time. The objective of a mammogram is to produce detailed images of the internal structures in breast tissue to make earlier cancer detection. Due to the need of details, high quality spatial images are required because the X-ray attenuation between normal and abnormal tissue is very small. Conventional mammogram uses film-screen detectors to record the photons that go through breast tissue, and it produces an analogical image. Due to the large amount of data that need to be stored, a piece of film is an excellent storage medium. Unfortunately, it is not possible to perform modifications in the image to improve the visualisation of present elements. In order to overcome the intrinsic limitations of conventional mammograms the use of digital mammograms is desirable. One of the fundamentals benefits of a digital mammogram is the facility to modify the image information. There are several kinds of lesions in breast tissue that can be detected in a mammogram, viz [9].

1. Primary signs:

- Dominant mass: This lesion is frequently found by analysing mammogram information. The lesion fall into one of four categories: benign, probably benign, probably malignant, and malignant.
- Dashed lesions (architecture alteration): Distorted areas of breast architecture with irregular edges that adopt a radiated morphology indicate an earlier sign of cancer but it is difficult to diagnostic.
- Microcalcifications: Frequently discovered and the analysis of its characteristics permits to differentiate a benign lesion from suspicious and clearly malignant lesions.

2. Secondary signs:

- Skin enlarger: Caused by lymphatic congestion and edema.
- Vascularisation increase: Due to cellular needs by cell proliferation.
- Lymphatic affectation: Due to permeability changes in lymphatic vases.
- Ductal dilation: Because liquid excess is present at the breast tissue.

2.1 Microcalcifications

Breast calcifications are commonly discovered in the radiological study on asymptomatic women. These are deposits of calcium at the thickness of mammary tissue and are represented as little white dots, and normally show the first sign of cancerous process. The main characteristics to determine the level of MCs abnormality are [9]

- i. Size: Larger than 2mm are classified as macrocalcifications and are usually benign. Microcalcifications are under 2mm length and are suspicious of malignant when they are small and grouped.
- ii. Morphology: Malignant calcifications usually are heterogeneous in form and size, namely, pointed, angular, and irregular, in “comma”, graft and with form of

point and ray. The benign ones usually are homogenous, round, and sometimes annular and with clear centre.

- iii. Quantity: A suspect of malignity is considered when there are five or more calcifications less to 1mm into an area of 1cm².
- iv. Distribution: Segmental distribution of calcifications, not random distribution, is indicative of biopsy.
- v. Calcification time variance: Stable calcifications into a period of 1.5-2 years are benign whereas malignant calcifications vary in time.
- vi. Calcifications associated with breast tissue: These are the first sign of breast cancer in young women.

Figure 1 shows different types of grouped MCs and an example of mammogram with MCs grouped linearly is shown in Figure 2.

2.2 MIAS database

In order to assess the performance of the proposed approach the mammography image analysis society (MIAS) database is used [9]. Table 1 shows the available information at the database for each mammogram that includes type of tissue, kind of abnormality, and strictness. In this paper only mammograms classified as CALC and NORM are analysed. Regarding the database some considerations should be noted [9]:

- The list of images is presented in pairs: even numbers correspond to left breast mammogram and odd numbers correspond to right breast mammogram as shown in Figure 3.
- The size of each image is 1024 × 1024 pixels and it is centred in the matrix.
- Coordinate system origin is at the bottom-left corner of mammogram.
- If microcalcifications are present, centre and radii are applied to a group of MCs not individually.
- In the case of MCs distributed into image and not concentrated, columns 5 and 6 are empty due to inappropriate coordinates and radii.

Examples of mammograms with several types of tissue are shown in Figure 4. It can be observed that the abnormalities in the mammogram are difficult to observe when there is an increment of changes into density tissue.

2.3 Wavelet transforms

The wavelet transform (WT) is a mathematical tool that provides building blocks with information in scale and in time of a signal [10]. These building blocks are generated from a single fixed function called mother wavelet by translation and dilation operations. The most commonly used mother wavelets are Haar, Daubechies, Mexican Hat, Morlet, and Walsh [10]. The process of wavelet transform of a signal is called analysis, and the inverse process to reconstruct the

analysed signal is called synthesis. The analysis generates different subband blocks (multi-resolution analysis, MRA [10]), so different resolution levels can be generated, as the application requires. This process is also known as subband coding [11]. The discrete wavelet transform (DWT) is a time-scale representation of a digital signal obtained with digital filtering techniques. The signal to analyse is passed through several filters with different cut-frequencies at different scales [10]. The wavelet family is generated by a mother wavelet $\psi(x)$ defined by [10, 16]

$$\psi_{j,k}(x) = \frac{1}{\sqrt{a_j}} \psi\left(\frac{x - b_k}{a_j}\right) \quad (1)$$

where a_j denotes the scale parameter, b_k represents the translation parameter, the term j controls scale and the term k controls translation. Further details on the DWT can be found in [10, 16]. The two-dimensional discrete wavelet transforms analyses digital images by separation of rows and columns, in this way the horizontal, vertical, and diagonal details are separated. In the first stage, the rows of an image $N \times N$ are filtered by one-dimensional (1D)-DWT analysis and then the same process is applied to the columns [15]. The previous process generates three different detailed sub-images HH, HL and LH. These correspond to three different directions (diagonal, vertical and horizontal, respectively) and a sub-image LL, known as approximation matrix, is used to the multi-level decomposition process. To reconstruct the image through the sub-images results of two-dimensional-DWT, details are recombined with the low-pass approximation and the up-sampling process. Note that the DWT is the non-redundant and compact representation of a signal in the wavelet domain. The down-sampling process makes the DWT time variant and produces shifting. The DWT is a powerful tool, although it has three main disadvantages that limit the performance in image processing applications, namely [13],

- Shift sensibility: It is derived from the down-sampling process because DWT coefficients fail to identify the shift in the input signal.
- Low directionality: The horizontal (LH), vertical (HL) and diagonal (HH) orientations are not enough to process the soft contours and random edges in natural images.
- Information inexistence about phase: A DWT application uses filters with real coefficients to process an image, so it is not possible obtain phase information.

The stationary wavelet transform (SWT) is the redundant, non down-sampling and full time invariant version of WT. The SWT has the same length of wavelet coefficients for each decomposition level. Furthermore, the SWT does not have sensibility but it is computationally complex. The computational complexity of the SWT is $O(n^2)$, where n denotes the length of samples in the signal [13]. The redundant representation of SWT does not present shifting. This is ideal for applications as contour detection, noise reduction, and data fusion [13].

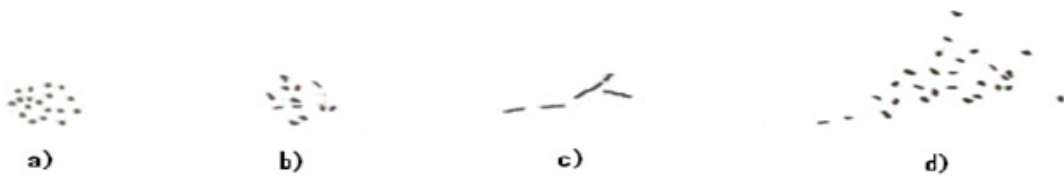


Figure 1 Types of MCs, a) and b) Grouped or clusters MCs. c) Linear MCs. d) Linear MCs & clustered.

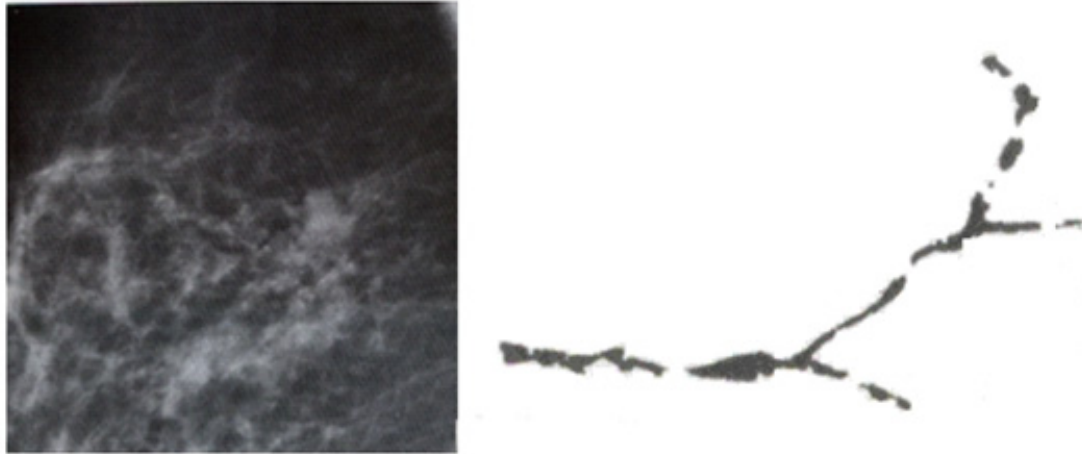


Figure 2 Image of mammogram with linear MCs.

Table 1 Mammogram information format [9].

mdb209 G CALC M 647 503 87		
1 st column	2 nd column	3 rd column
Reference number from MIAS database. The database includes 322 mammograms.	Type of tissue: F-Fatty, G- Fatty-Glandular, D-Dense-Glandular.	Class of abnormality: CALC-Calcification, CIRC-Circumscribed masses, SPIC-Spiculated masses, MISC-other, ill-defined masses, ARCH Architectural distortion, ASYM- Asymmetry, NORM-Normal.
4 th column	5 th & 6 th column	7 th column
Severity of abnormality: B-Benign, M-Malignant	(x, y) image-coordinates of centre of abnormality.	Approximate radius (pixels) of a circle enclosing the abnormality.

2.4 Complex wavelet transform (CWT)

The complex wavelet transform (CWT) is used to avoid the limitations of DWT and to obtain phase information. The CWT employs a complex value filtered analytically to decompose pure real signals and real signals with complex components into real and imaginary parts in the wavelet domain. Real and imaginary coefficients are used to compute amplitude and phase information, needed to describe precisely the energy localisation of oscillating sources. Recent investigations in the CWT field are addressed to the design of complex filter banks, in which the outputs are wavelet coefficients (real and imaginary). It is desirable that filters form pairs of Hilbert transform on each decomposition level. The CWT is classified into two groups, namely, the Redundant-CWT (RCWT)

and the Non-redundant-CWT (NR-CWT), and it is a powerful tool to image compression [13].

2.4.1 Analytical filters

The Hilbert transform was introduced for signal processing by Gabor. It is defined as an extension of a real signal $s(x)$ according to

$$r(x) = s(x) + i g(x) \quad (2)$$

where $g(x)$ is the Hilbert transform of $s(x)$ denoted by $H\{s(x)\}$ and $i = (-1)^{\frac{1}{2}}$ [13]. The signal $g(x)$ is the 90° shifted version of $s(x)$ as shown in Figure 5(a). The signal $g(x)$ is orthogonal to $s(x)$. If $S(\omega)$ is the Fourier Transform (FT) of signal $s(x)$ and $G(\omega)$ is the FT of $g(x)$, the relation

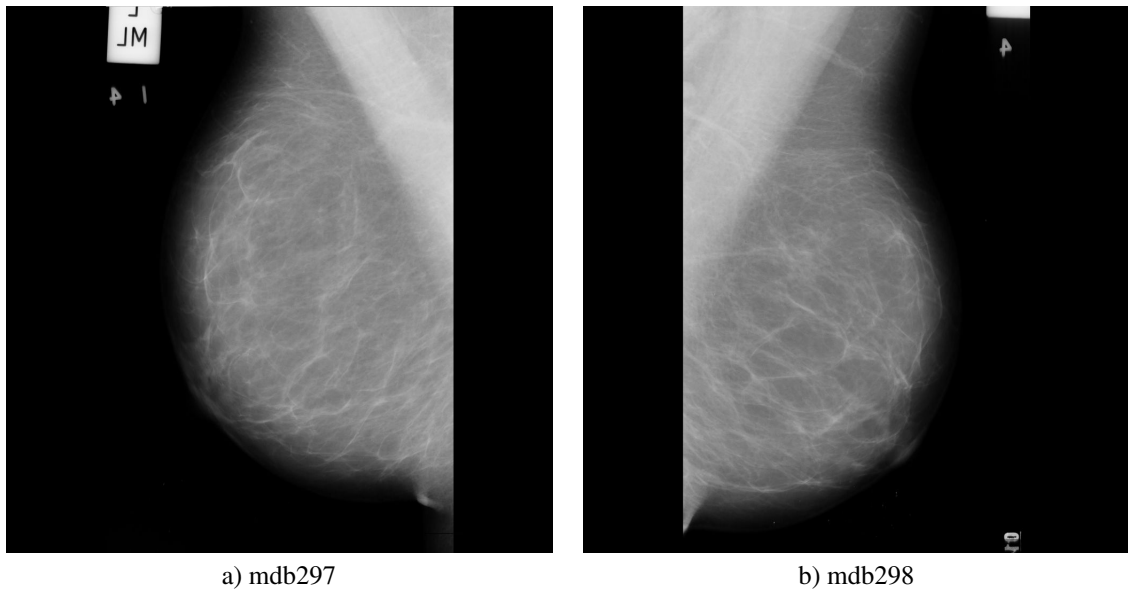


Figure 3 (a) Mammogram corresponding to right breast and (b) Mammogram corresponding to left breast.

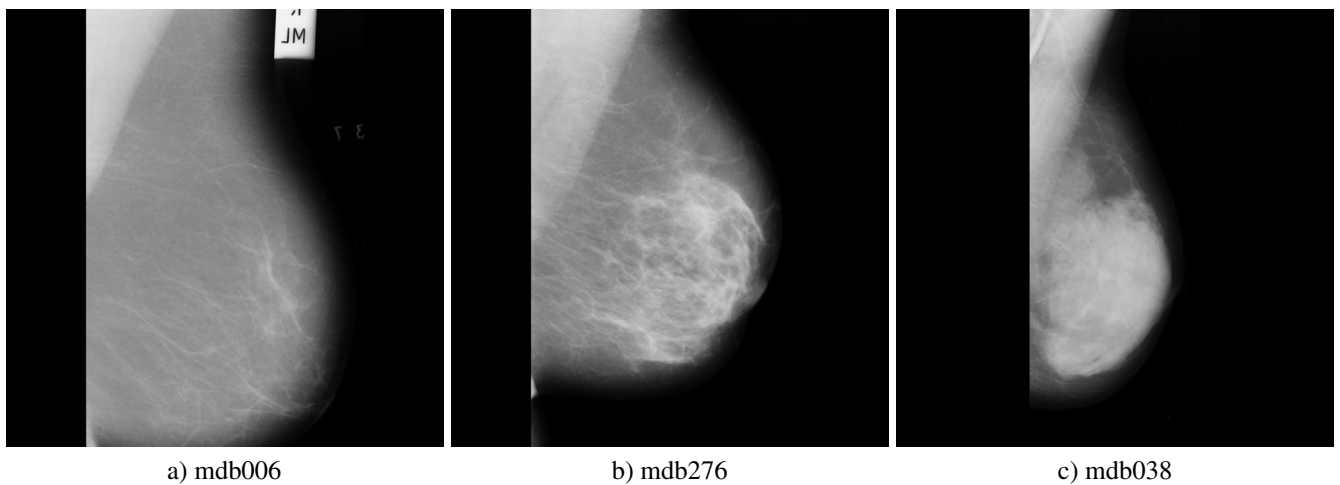


Figure 4 Mammograms with several densities of tissue: (a) Fatty (F), (b) Fatty-Glandular (G), and (c) Dense-glandular (D) according to the MIAS database.

between $s(x)$ and $g(x)$ in the frequency domain is given by

$$G(\omega) = S\{H\{s(x)\}\} = -i \text{Sgn}(\omega)S(\omega) \quad (3)$$

where $-i\text{Sgn}(\omega)$ is the modified signum function shown in Figure 5(b). In the time domain, $g(x)$ can be represented by [13]

$$g(x) = H\{s(x)\} = \frac{1}{\pi} \int_{-\infty}^{\infty} \frac{s(x)}{x - \tau} d\tau = s(x) \frac{1}{\pi \tau} \quad (4)$$

where τ denotes the integration variable. The estimate of instantaneous frequency and amplitude of signal $r(x)$ are given by

$$\begin{aligned} \text{Magnitude of } r(x) &= \sqrt{s(x)^2 + g(x)^2} \\ \text{Angle of } r(x) &= \tan^{-1} \frac{g(x)}{s(x)} \end{aligned} \quad (5)$$

The previous quadrature representation results in a non-negative spectral representation in the Fourier domain that

uses only a half of the bandwidth, this decreases the “aliasing”. Reduction of the “aliasing” is the key for shift insensibility of CWT. Figure 6 shows the frequency spectrum of an original signal $S(\omega)$ and its analytic representation $R(\omega)$. The previous concept is applied to a filter bank of the DWT to produce complex solutions that originates the CWT. Real coefficients are replaced by complex coefficients. The complex filter can be decomposed into two real filters (seen Figure 7). The impulse response of each filter constitutes the Hilbert pairs. The combination of these filters is known as analytic filter.

2.5 Redundant complex wavelet transform (RCWT)

The RCWT is presented in two variants, namely, the dual-tree complex wavelet transform of Kingsbury (DT-CWT (K)) and the DT-CWT of Selesnick (DT-CWT (S)). Both of them are redundant due to a similar filter bank structure with the DWT, but in this case the banks operate in parallel and in quadrature.

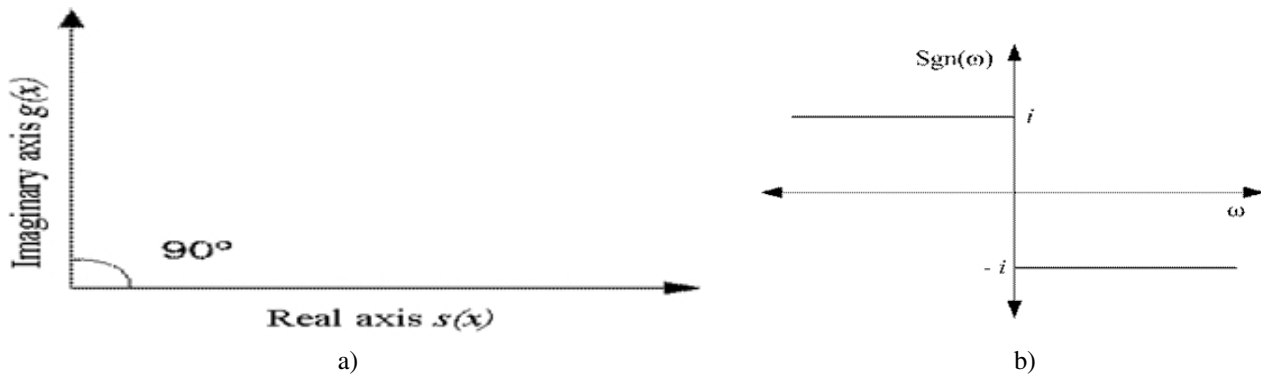


Figure 5 Hilbert transform a) polar form, b) frequency domain.

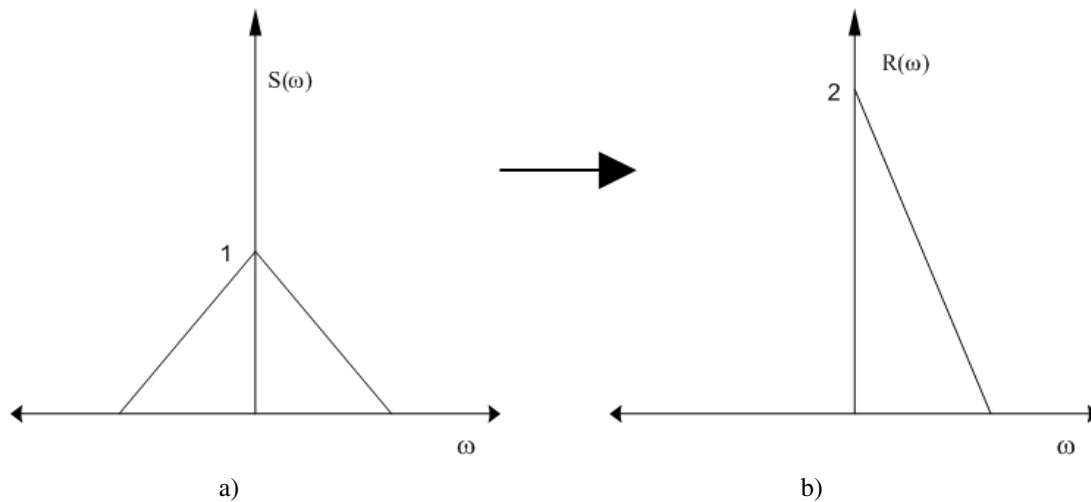


Figure 6 Spectral representation a) original signal $s(x)$ b) analytic signal $r(x)$.

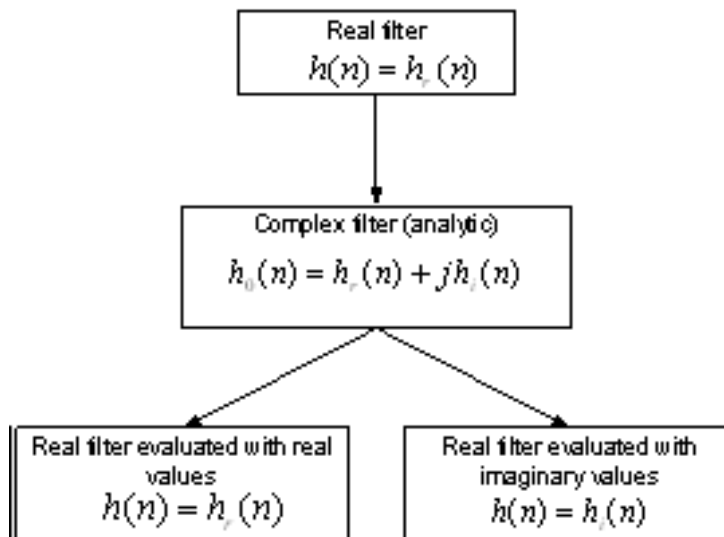


Figure 7 Interpretation of an analytic filter into two real filters [13].

The filter structure is the same in both variants; the difference is the method that generates the wavelet and scaling coefficients. Both DT-CWT variations generate phase information, are insensitive to shifting, and are directional. The CWT follows the same principle of DWT, and at the output there are the same number of samples n that at the input. Furthermore, the computational complexity is only twice of the DWT, $O(2n)$

[13]. Although, both DT-CWT have the same filter bank structure of DWT, the difference is that analytical filters replace real filters in order to obtain complex solutions. It is similar of two parallel filter bank structures in the DWT [13, 17]. Figure 8 shows the filter bank structure to DT-CWT analysis at three level of decomposition in one-dimension. The form of the conjugated filters for one-dimensional DT-CWT is defined by

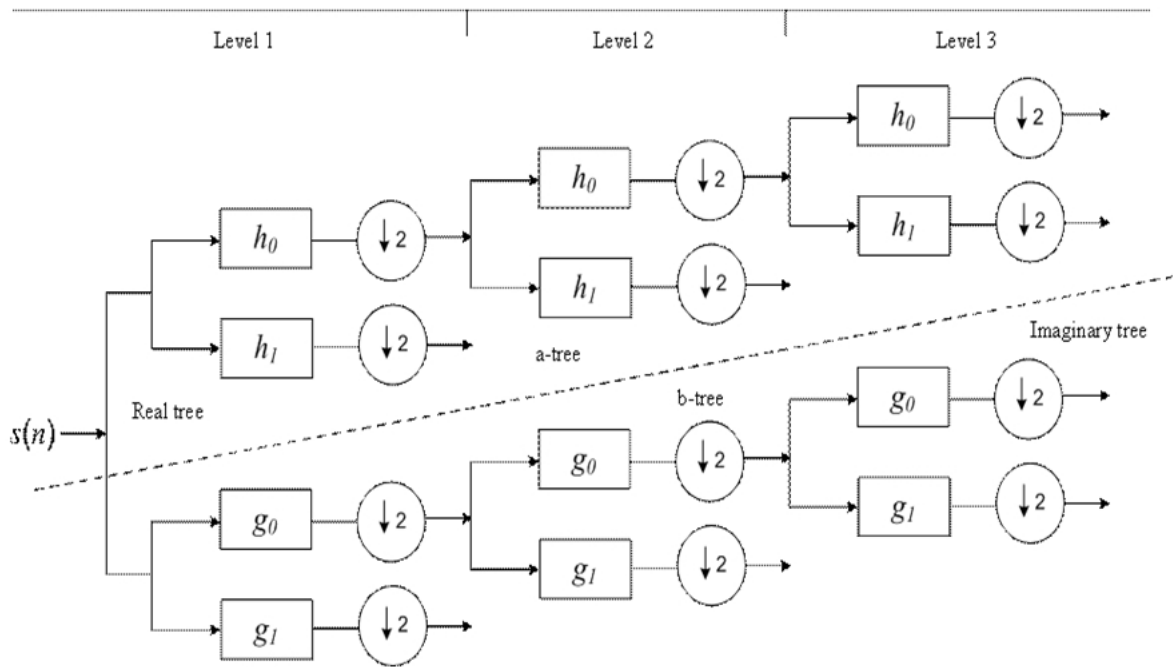


Figure 8 Analysis filter bank for 1D DT-CWT.

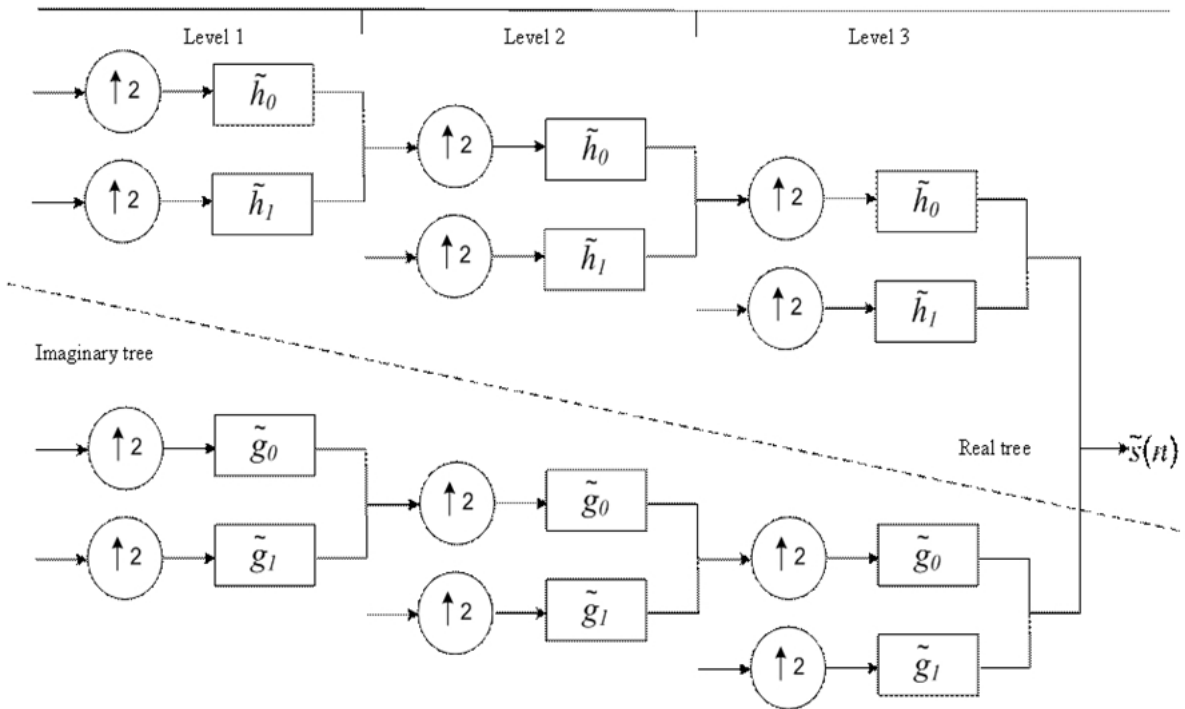


Figure 9 Synthesis filter bank for 1D DT-CWT.

$$(h_n + i g_n) \tag{6}$$

where h_n is the set of filter $\{h_0, h_1\}$ and g_n is the set $\{g_0, g_1\}$. Filter h_0 and h_1 correspond to low-pass and high-pass filter respectively for real tree, in the same way filter g_0 and g_1 are in the imaginary tree. It should be noted that notation h_0 and h_1 for real tree (a-tree) and g_0 and g_1 for imaginary tree (b-tree) is used in entire trees, but numerical values for each filter

differs from the other at each level. The synthesis filter bank is shown in Figure 9. The reconstruction process is realised with the pairs \tilde{h}_0, \tilde{h}_1 and \tilde{g}_0, \tilde{g}_1 . In Figure 10, it is shown the structure for a two-dimensional (2D) implementation; in this case there are four trees for signal analysis and synthesis. The pair of complex filters is applied in 2-D (m, n) , where m and n denote de elements of a two-dimensional array that can be expressed as follows:

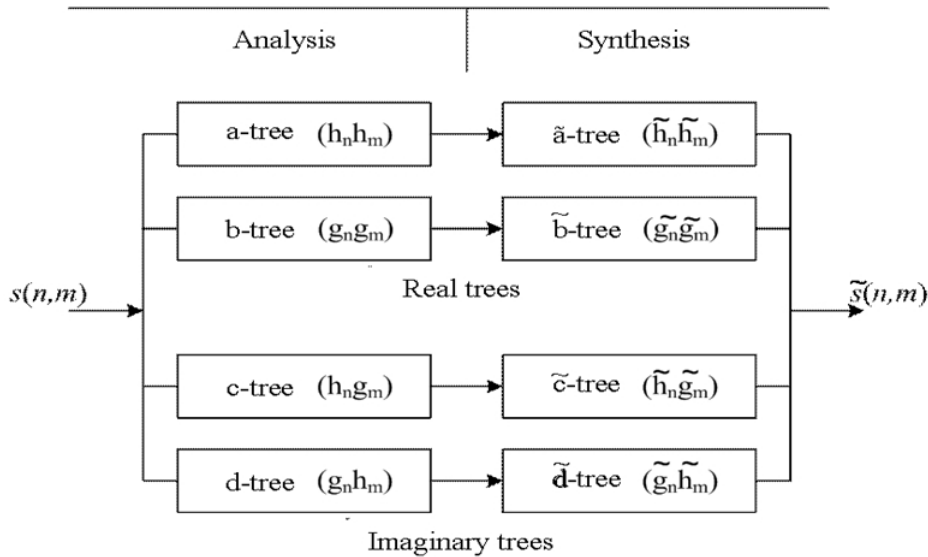


Figure 10 Filter bank structure for 2-D DT-CWT.

$$(h_n + i g_n)(h_m + i g_m) = (h_n h_m - g_n g_m) + i(h_n g_m - g_n h_m) \quad (7)$$

The pair constituted by a & b tree are the real part whilst c & d tree are the imaginary part. In order to reconstruct the signal trees $\{\tilde{a}, \tilde{b}\}$ are used for real part and trees $\{\tilde{c}, \tilde{d}\}$ for imaginary parts. In the work reported in this paper the DT-CWT(S) is employed to detect microcalcifications. The DT-CWT(S) uses either the Grobner's bases or spectral factorization method for the design of analytical quadrature filters for one dual-tree. The DT-CWT(S) design probes for the two orthogonal wavelets that conforms the Hilbert transform, the scaling filters should be at an offset level of $1/2$ sample. Equation (8) represents mathematically the filter bank structure (see Figure 8) with conjugate quadrature filters (CQF) pair h_0 and h_1 .

$$\sum_n h_0(n)h_0(n+2\ell) = \delta(\ell) = \begin{cases} 1 & l = 0 \\ 0 & l \neq 0 \end{cases} \quad (8)$$

$$h_1(n) = (-1)^{(1-n)}h_0(1-n)$$

Equations for scaling $c_h(x)$ and wavelet coefficients $d_h(x)$ of real part are defined by

$$c_h(x) = \sqrt{2} \sum_n h_0(n)c_h(2x-n) \quad (9)$$

$$d_h(x) = \sqrt{2} \sum_n h_1(n)d_h(2x-n) \quad (10)$$

Correspondingly, imaginary part coefficients c_g and d_g are defined similarly for the imaginary tree. In order to generate the Hilbert transform the filters are different at each decomposition level. Reconstruction filters are the inverse version of the transformation filters. Further details can be found in [13, 17].

2.5.1 Properties of DT-CWT

The DWT and the DT-CWT have similar properties due to identical filter structure. The properties of the DT-CWT are [17]:

- **Shift insensibility:** reconstructed detail at last level has almost the same shifting present in original signal. This allows that the DT-CWT has successful results in applications as motion estimation on images and image fusion at different resolution levels.
- **Directionality:** The DT-CWT has six directions, three for real part and three for imaginary part oriented at $\pm 15^\circ$, $\pm 45^\circ$ and $\pm 75^\circ$ in case of images.
- **Phase information:** This is due to the two parallel trees of the DT-CWT. Phase can be computed at each level with real and imaginary parts. The one-dimensional complex wavelet is an envelope of real and imaginary wavelets in quadrature (Hilbert pair) as shown in Figure 11 [13].
- **Reconstruction:** The DT-CWT reaches the conditions of perfect reconstruction.
- **Redundancy:** The redundancy is 2:1 or $2^J:1$, where J denotes the maximum number of decomposition levels. In this regard, the DT-CWT is more expensive than the DWT but less than the SWT.

3. PROPOSED APPROACH

In this section we report an approach to detect microcalcifications in digital mammograms using the DT-CWT (S). The DT-CWT has shown a good performance in applications that involve image processing due to more data phase information, shift invariance, and directionality than other wavelet transforms. The approach consists of four stages, namely,

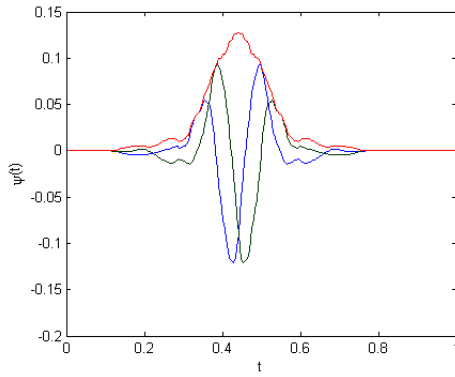


Figure 11 1-D Complex wavelet resulting from quadrature combination of real and imaginary wavelets [13].

image denoising by optimal thresholding, suppression of low-band frequencies, morphological transformation, and inverse complex wavelet transform. Microcalcifications are small deposits of calcium that appear as diminutive white dots in the mammogram. Due to size of microcalcifications, the non-homogeneous background of mammogram (breast glandular tissue) and noise present, detection of MCs is difficult [6]. The approach reported in this paper assumes that MCs present in mammograms can be obtained using a transform that locate image characteristics into the wavelet transform domain. The WT allows the multi-resolution analysis and image decomposition in subband frequencies in which the low-band frequencies are image background and high-band frequencies correspond to image details. MCs correspond to the high-band frequencies of mammogram spectrum [5]. Figure 12 shows the block diagram of the proposed approach. The five steps that conforms the approach to detect MCs are 1) Mammogram sub-band frequency decomposition, 2) Mammogram noise reduction, 3) Suppression of bands containing low frequencies, 4) Dilation of high frequency components and 5) Mammogram reconstruction.

3.1 Mammograms sub-band frequency decomposition

The original mammogram is decomposed into a subband set, each band with different resolution and frequency contents. This process is performed with the DT-CWT proposed by Selesnick (see Section 3.2). There are two variants of the DT-CWT(S), the DT-CWT (real) and the DT-CWT (complex). Both of them have wavelets oriented in six directions. The difference is that the DT-CWT (complex) uses two wavelets for each direction, one interpreted as the real part and the other as the imaginary part. Due to the complex version there are double numbers of wavelets than the DT-CWT (real). The DT-CWT (complex) is four times expansive and the DT-CWT (real) is two times expansive [13]. The complex wavelet transform used in this work to detect MCs is the DT-CWT (real). The DT-CWT has six different wavelets oriented at $\pm 15^\circ$, $\pm 45^\circ$, and $\pm 75^\circ$ for $i = 1, 2, 3$ as follows [13, 17]:

$$\psi_i(n, m) = \frac{1}{\sqrt{2}}(\psi_{3,1}(n, m) + \psi_{4,i}(n, m)) \quad (11)$$

$$\psi_{i+3}(n, m) = \frac{1}{\sqrt{2}}(\psi_{3,1}(n, m) - \psi_{4,i}(n, m)) \quad (12)$$

Oriented wavelets are produced from 2-D wavelets $\psi(n, m) = \psi(n) \psi(m)$ associated with row-column implementation of wavelet transform, where $\psi(n)$ is the complex wavelet defined by

$$\psi(n) = \psi_h(n) + j \psi_g(n) \quad (13)$$

where h and g denote the corresponding low-pass and high-pass filters respectively. Thus, the oriented wavelets are [17]

$$\psi_{3,1}(n, m) = \phi_g(n) \psi_h(m) \quad (14)$$

$$\psi_{3,2}(n, m) = \psi_g(n) \phi_h(m) \quad (15)$$

$$\psi_{3,3}(n, m) = \psi_g(n) \psi_h(m) \quad (16)$$

$$\psi_{4,1}(n, m) = \phi_h(n) \psi_g(m) \quad (17)$$

$$\psi_{4,2}(n, m) = \psi_h(n) \phi_g(m) \quad (18)$$

$$\psi_{4,3}(n, m) = \psi_h(n) \psi_g(m) \quad (19)$$

3.2 Mammogram noise reduction

The noise reduction in the mammogram is realised into transform domain by an optimal threshold algorithm that modifies the signal representation coefficients according to each decomposition level. The method used to obtain the optimal threshold consists in the stages of initialisation, iteration, and convergence [19]. The main objective is to implement a method to remove image noise using a non-linear and recursive algorithm called optimal threshold algorithm with CWT theory. Threshold application on wavelet coefficients is an efficient method for noise removal in a signal [20]. A quasi-optimal threshold method depends upon sampled signal length and noise variance that generally is an unknown parameter. In this section, a recursive method to estimate noise variance is presented. The threshold limit depends on the probability density function (PDF) of noise. In order to obtain the threshold in this recursive method two values are calculated to initialise the process, viz [20].

A. Initialisation

The values that should be obtained are the variance of noised signal σ_0^2 and the initial threshold λ_0 . The methodology to obtain these values is as follows:

- Given the sampled noised signal $p(n)$ with n denoting the number of signal samples, the discrete or complex wavelet transform is calculated to obtain \hat{p}_γ , where γ is a multiple index $\gamma = (j, k)$, with j and k denoting scale and wavelet position respectively. Note that in a bi-dimensional signal n is substituted by $n \times m$.

When wavelet signal decomposition is obtained, the noise variance of transformed signal is computed by using

$$\sigma_0^2 = \frac{1}{n} \sum_{\gamma \in \Gamma^J} |\hat{p}_\gamma|^2, \quad (20)$$

where Γ^J is a set of indexes defined by $\Gamma^J = \{\gamma(j, k), j = 0, \dots, J-1, \& k = 0, \dots, 2^J-1\}$ [19]. The threshold λ_0 is computed by using $\lambda_0 = (2 \ln n \sigma_0^2)^{1/2}$.

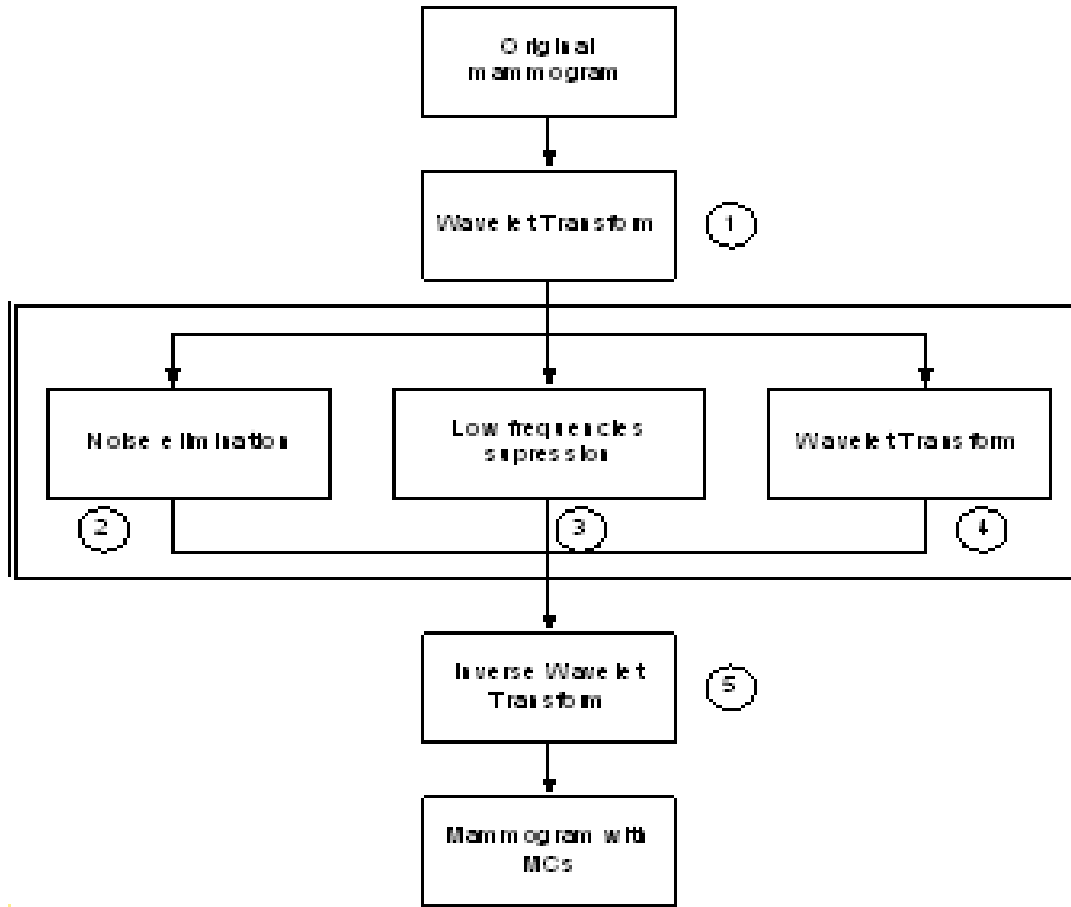


Figure 12 Block diagram of proposed approach to detect MCs.

B. Iteration

- New variance and threshold values are calculated $\sigma_{t+1}^2 = \frac{1}{n} \sum_{\gamma \in \Gamma^J} |\hat{p}_\gamma, \lambda_0|^2$ and $\lambda_{t+1} = (2 \ln n \sigma_{t+1}^2)^{1/2}$ [20].
- With a defined sequence of estimated thresholds $(\lambda_t)_{t \in T}$ and estimated variances $(\sigma_t^2)_{t \in T}$ the convergence of the new values depends upon initial value and iteration function $I_{p,n}(\lambda)$.

$$I_{p,n}(\lambda) = \left(\frac{2 \ln n}{n} \sum_{\gamma \in \Gamma^J} |(\hat{p}_\gamma, \lambda_t)|^2 \right)^{1/2} \quad (21)$$

$$= \left(\frac{2 \ln n}{n} \sum_{\gamma \in \Gamma^J} |(\hat{p}_\gamma)|^2 \right)^{1/2} \quad (22)$$

(23)

C. Convergence

To get a fixed threshold estimation, it is necessary to consider the following:

- The defined iteration function $I_{p,n}(\lambda)$ supposes the existence of an interval $[\lambda_a, \lambda_b]$ in which $I_{p,n}(\lambda_a) \geq \lambda_a$ and $I_{p,n}(\lambda_b) \leq \lambda_b$; in addition, the existence of a step t_0 in which $\lambda_{t_0} \in [\lambda_a, \lambda_b]$, then in general form, $\lambda_t = I_{p,n}(\lambda_{t-1})$ converges to a limit threshold value λ_{li}

contained in $[\lambda_a, \lambda_b]$. This is demonstrated in [20], and permits to obtain a threshold $\lambda_{li} = I_{p,n}(\lambda_{li})$.

$$\lambda_{li} = I_{p,n}(\lambda_{li}) = \left(\frac{2 \ln n}{n} \sum_{\gamma \in \Gamma_{\lambda_{li}}} |\hat{p}_\gamma|^2 \right)^{1/2} \quad (24)$$

The thresholds values are obtained for each decomposition level and are not dependant of a proposed variance but from the variance estimation of signal noise. Equation (22) is defined for a one-dimensional signal; the 2-D extension is obtained by substituting n with $(n \times m)$. To reduce noise in digital mammograms by considering the CWT extracted coefficients and applying the optimal threshold, the following points should be considered:

- The first stage consists in decomposition of the noised signal into wavelet coefficients using the complex wavelet transform.
- A threshold level is then obtained with the assistance of the optimal threshold algorithm [20]. This procedure modifies the wavelet coefficients in distinct form for each decomposition level of the CWT.
- Finally, the reconstruction process is realised with the modified coefficients.

3.3 Suppression of bands containing low frequencies

To eliminate mammogram background that difficult visibility of MCs the suppression of bands that contain mammogram low-band frequencies is performed. This objective is achieved by scaling coefficient suppression from real and imaginary part of DT-CWT(S), defined in Equation (9), then

$$c_h(x) = \sqrt{2} \sum_n h_0(n) c_h(2x - n) = 0 \quad (25)$$

3.4 Dilation of high frequency components

It is necessary to stand out the subbands components that contain high frequencies in which MCs are present. This is achieved by a morphological operation of dilation. The result of dilation is the set of origins points of the structuring element Y in which the structuring element contains some element from X set when the element is displaced through the space that contains both sets. The equation that models dilation $\delta_Y(X)$ is given by [3, 6]

$$\delta_Y(X) = \{x | Y_x \cap X \neq \emptyset\} \quad (26)$$

where X is a pixel set, Y is a structuring element (with circle, triangle or hexagonal shape) and x is the set of pixels concerned to X . The wavelet coefficients contain image details so it is necessary to dilate each of six oriented bands; thus $\delta_Y(\psi_i(x, y))$ for $i = 1, \dots, 6$. The used structuring element Y is a circle that contains the MCs.

3.5 Mammogram reconstruction

Finally, DT-CWT synthesis is applied to the filter bank as explained in Section 3.2 and the DT-CWT subbands, previously processed with the described methods of image denoising, low frequencies subband suppression, and high frequencies components dilation in which is obtained the mammogram that contains only the MCs.

4. EXPERIMENTAL RESULTS

To assess the performance of the proposed approach experimental results using the SWT and the top-hat transformation are also presented. The results after applying these methods in mammograms from the MIAS database are reported. The top-hat transformation is mainly employed for detail extraction in images. There are two kinds of top-hat transformation. The white top-hat transformation for brighten details extraction and the black top-hat transformation for dark details extraction [6]. Because MCs are present as bright particles rounded by a black background, then the white top-hat transformation is considered. The top-hat transformation consists on recovering the structures eliminated in the open or closed process. Using a structuring element with suitable shape, size and orientation it is possible to filter the image and eliminate particular elements of the original image. The white top-hat transform is the residue between original image and morphological open.

Equation (25) shows the definition of white top-hat filtering [3].

$$\rho(X) = \frac{X}{\gamma(X)} \quad (27)$$

where $\rho(\cdot)$ denotes the white top-hat transform and $\gamma(\cdot)$ is the open process or morphological dilation $\delta_Y(X)$. Furthermore, to compare the efficiency of the proposed approach simulations are first realised with mammograms using the DWT, the SWT, and the morphological top-hat filtering. In the SWT and the DWT case, the fourth order Daubechies (*db4*) wavelet is used. Other wavelets may also be considered.

4.1 MCs detection using DWT and SWT

The DWT disadvantages decrease its efficiency in digital image processing; in addition, when using the DWT for MCs detection the inconvenient is the down-sampling process that eliminates details in the image, especially when MCs are details in high-band frequencies. Figure 13 shows the results of applying a four level decomposition DWT to a mammogram with the wavelet Daubechies 4 (*db4*). Note that the detection of MCs using the SWT and the DWT is accomplished by setting low frequencies subbands to zero, and before image reconstruction the universal threshold algorithm with a soft threshold is applied at each level of wavelet decomposition [22]. It can be seen that the DWT is not a good alternative for MCs detection because the down-sampling process makes the DWT time variant. The SWT is the non-redundant, non-down-sampling and fully time-invariant version of WT. The coefficients length of the SWT is the same at each decomposition level and it has a similar structure to the DWT without down-sampling. The redundancy of the SWT avoids shifting. This is ideal for edge detection, noise reduction, and data fusion. The SWT increases significantly MCs detection to overcome the DWT disadvantages. In Figure 14(a) a mammogram with MCs is shown. The image obtained after applying a four level decomposition SWT with *db4* is shown in Figure 14(b). It can be seen that the performance of the SWT is better than the performance of the DWT because it detects the MCs. However, the SWT process fails because it also shows glandular tissue. Furthermore, its high redundancy increments the computational complexity to $O(n^2)$ [13]. In order to overcome the limitations of the DTW and the SWT we use the DT-CWT.

4.2 Comparative results

Figure 15 shows an original mammogram called **mdb233 G CALC M *NOTE 3***. According to Table 1 this mammogram corresponds to a Glandular tissue (G) and contains a set of malignant MCs. NOTE 3 denotes that when calcifications are present, centre locations and radii are applied to a group of MCs rather than individually. As can be seen in Figure 15, when using the SWT the MCs (brighten points) are appreciable, but its visibility is difficult because other image details appear (tissue and breast glands), and the computational complexity is high, $O(n^2)$. With the proposed approach using the DT-CWT better results are obtained. MCs are more visible and other objects presented by the SWT disappear; in

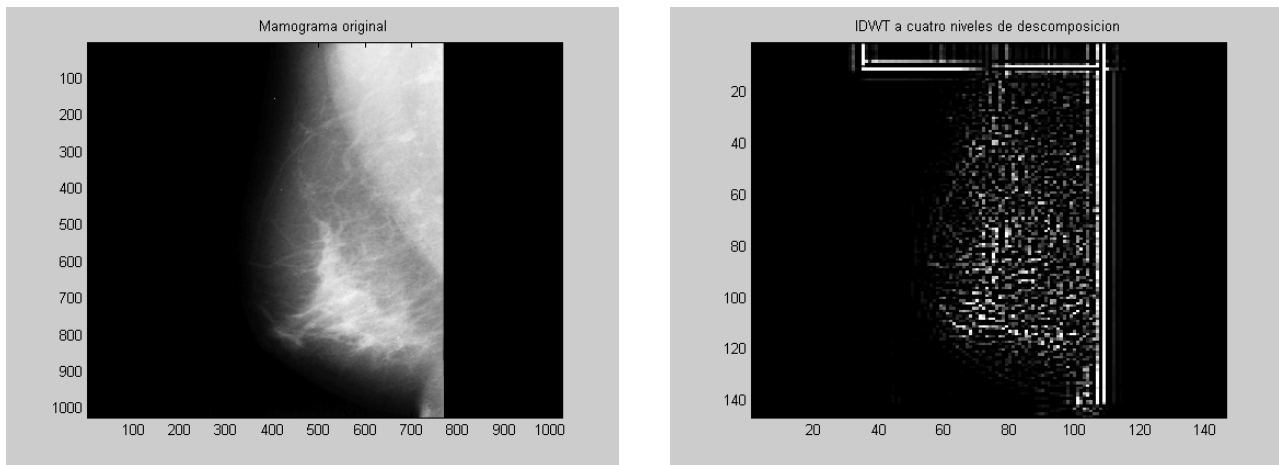


Figure 13 MCs detection using a four level decomposition DWT. [left] Original mammogram and [right] Image obtained after applying IDWT process.

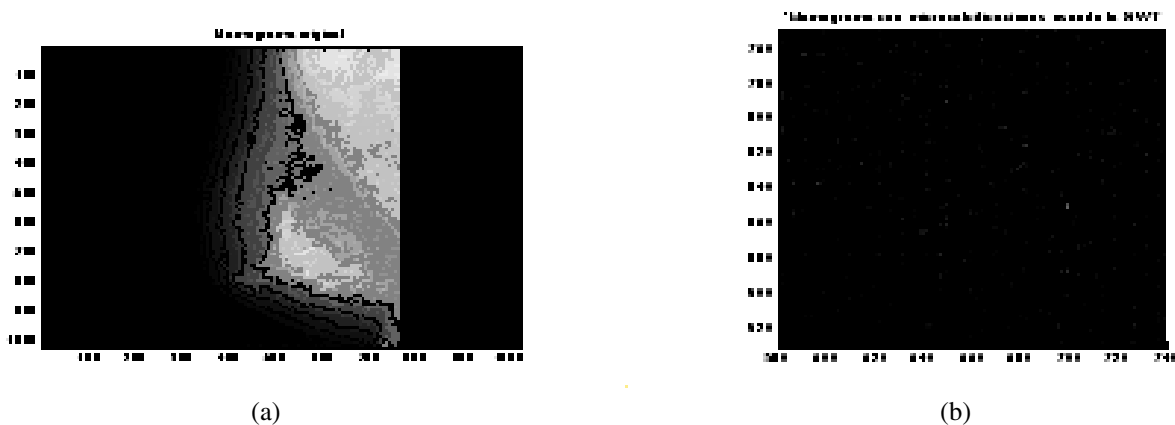


Figure 14 MCs detection using four levels of decomposition SWT, (a) Original mammogram, (b) Image from ISWT process.

addition the DT-CWT has lower computational complexity, $O(2n)$. The results obtained with the top-hat transformation show that this is the worst method to detect MCs. This is due to the fact that other tissue and breast glands are not filtered and appear together with MCs, which are not significantly appreciated as in the cases of the two other simulated methods.

Likewise, results are interpreted for the case of the mammogram **mdb249 D CALC M 544 508 48** shown in Figure 16. In this case a set of MCs are present at the approximate centre of image (544, 508) [9]. Yet again it is observed that using the DT-CWT a better detection of MCs without inherent mammogram characteristics is obtained. This is not possible with the SWT because there are not tissue and glandular filtering. Finally in Figure 17, experimental results are obtained from the mammogram **mdb003 D NORM**. This is a normal mammogram (without MCs presence). As can be observed on the SWT and the top-hat transformation results, tiny details are appreciated in the mammogram, whilst with the proposed approach a mammogram fully free of MCs and other details is obtained.

The aforementioned approaches were applied to a set of 15 mammograms of different types of tissue. Six mammograms of Glandular tissue (G), five of Dense-Glandular tissue (D) and four of Fatty tissue (F) were used. The results obtained by using the SWT and the proposed approach are in some

way similar (as can be seen in Figure 15 and in Figure 16), both of them detect MCs, but with the SWT some inherent characteristics of breast (tissue and glands) are not filtered. The detection criterion on Fatty tissue (F) to determine if a good detection was realised, is the presence of MCs without tissue or breast glands. This is reported in Table 2 with “1”, whilst it is considered a bad detection when in addition to MCs, other breast characteristics are filtered, and it is reported with “0”. In the cases of Dense-Glandular (D) and Glandular (G) tissues, the detection becomes difficult due to the tissue nature, so the symbol “0” represents that detection of MCs was not achieved. An important factor to consider is the type of tissue in the mammogram so that with Glandular (G) and Dense-Glandular (D) tissues, the detection becomes difficult, whilst the best results are obtained for Fatty tissue (F). Table 2 reports the results after applying the proposed approach, the SWT and the top-hat filtering on digital mammograms. From the fifteen analysed mammograms in the proposed approach ten of them were classified with a “1” then a detection rate of 66.6% was obtained, whilst the detection rate for the SWT and the top-hat filtering was 34% and 20% respectively. The low detection rate for the proposed approach is produced by the nature of Glandular (G) and Dense-Glandular (D) tissues. However, with Fatty tissue (F) better results are obtained, as can be observed in Table 2.

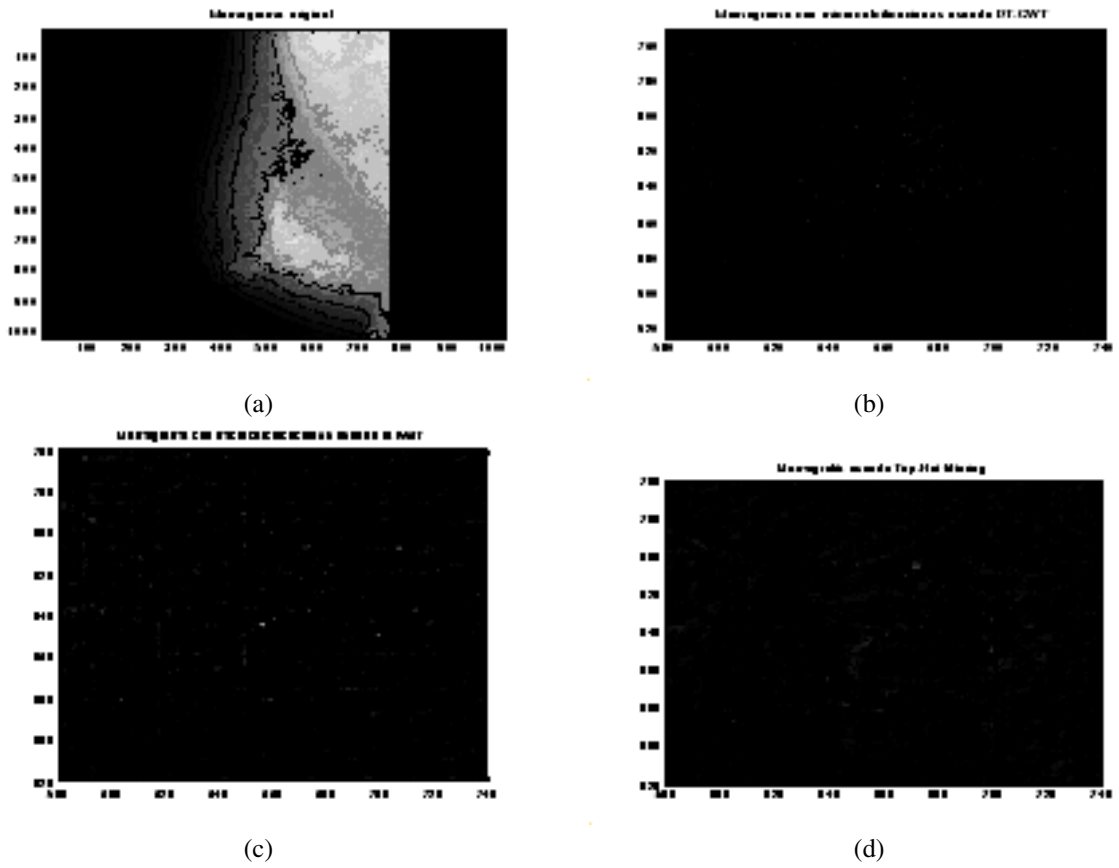


Figure 15 Experimental results for the mammogram mdb233 G CALC M *NOTE 3*. (a) Original mammogram, (b) Mammogram with MCs using the DT-CWT, (c) Mammogram with MCs using the SWT, and (d) Mammogram with MCs using the top-hat filtering.

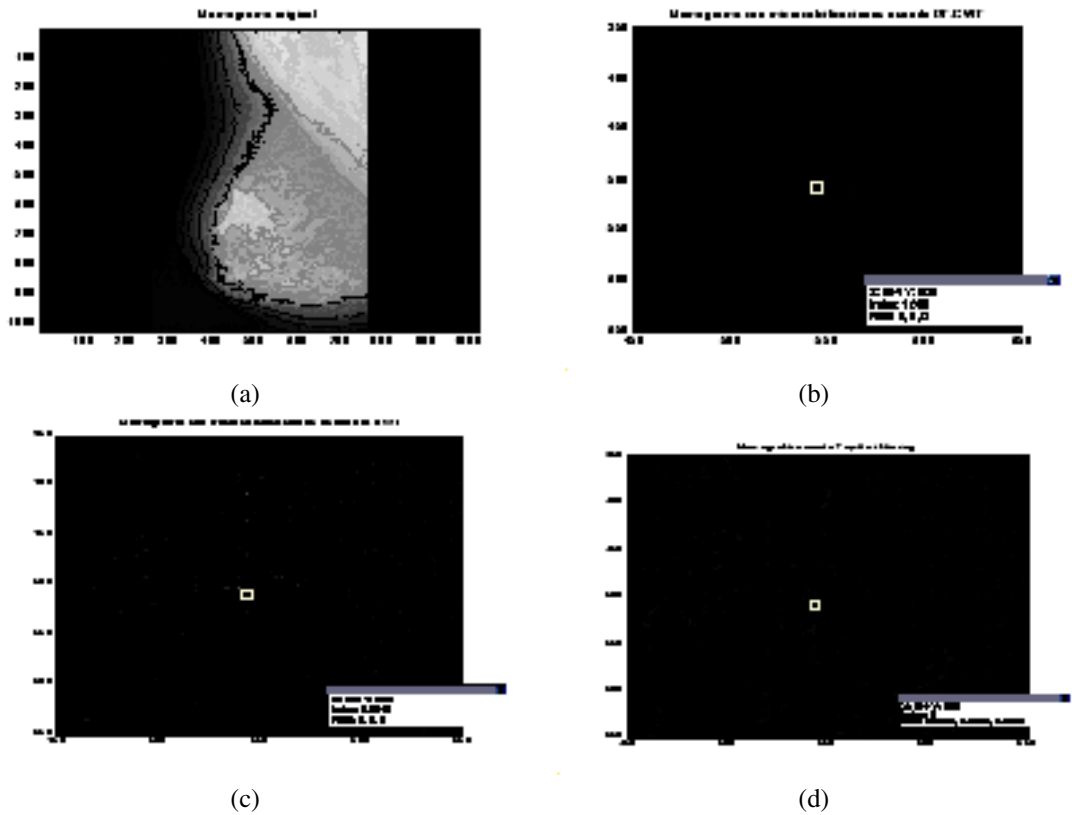


Figure 16 Experimental results for the mammogram mdb249 D CALC M 544 508 48. (a) Original mammogram, (b) Mammogram with MCs using the DT-CWT, (c) Mammogram with MCs using the SWT, and (d) Mammogram with MCs using the top-hat filtering.

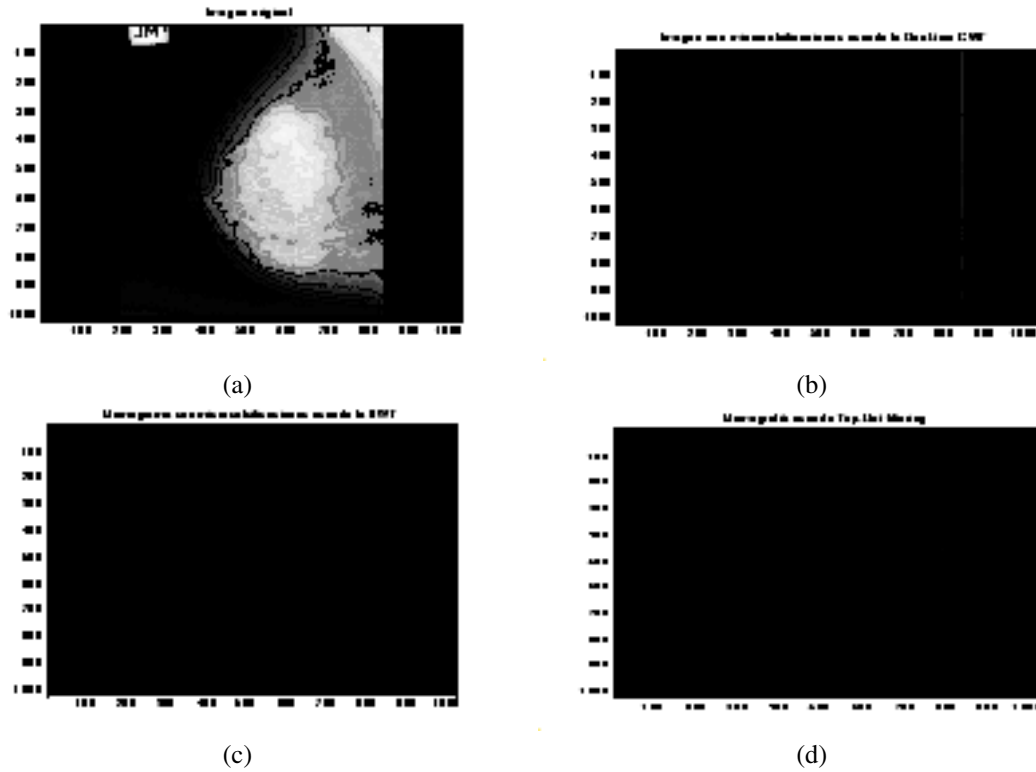


Figure 17 Experimental results for the mammogram mdb003 D NORM. (a) Original mammogram, (b) Mammogram with MCs using DT-CWT, (c) Mammogram with MCs using SWT, and (d) Mammogram with MCs using the top-hat filtering.

Table 2 Experimental results for the proposed approach, the SWT and the top-hat filtering, where G (Glandular tissue), D (Dense-Glandular tissue) and F (Fatty tissue). A good detection is represented with “1” and a bad detection with “0”.

MAMMOGRAM	Type of lesion	Type of tissue	DT-CWT	SWT	Top-hat
mdb209	CALC	G	1	1	0
mdb211	CALC	G	0	0	0
mdb213	CALC	G	1	1	1
mdb218	CALC	G	0	0	0
mdb219	CALC	G	1	0	1
mdb233	CALC	G	1	1	0
mdb216	CALC	D	0	0	0
mdb222	CALC	D	0	0	0
mdb223	CALC	D	1	1	1
mdb226	CALC	D	0	0	0
mdb249	CALC	D	1	1	0
mdb231	CALC	F	1	0	0
mdb238	CALC	F	1	0	0
mdb245	CALC	F	1	0	0
mdb252	CALC	F	1	0	0

5. CONCLUSIONS AND FUTURE WORK

In the work reported in this paper we have proposed an approach to detect MCs in digital mammograms using the DT-CWT. The approach consists of the DT-CWT application to obtain a mammogram subband decomposition, mammogram denoising by applying an optimal threshold at each decomposition level, suppression of mammogram low frequencies, application of morphological operators to enhanced MCs visualization, and finally, the reconstruction of the mammogram.

The results obtained using the DT-CWT are compared to the results obtained using the SWT and the top-hat transformations. The proposed approach shows the best performance to detect MCs in digital mammograms. The SWT detects the MCs but other details are also observed as MCs. Another inconvenient presented by the SWT is the computational complexity, $O(n^2)$, in contrast, the computational complexity of the DT-CWT is $O(2n)$ only. From results obtained morphological filtering is the worst method to detect MCs, because MCs are not well appreciated. Furthermore, tissue and breast

glands are presented in the reconstructed mammogram. It is also observed that the results have variation that depends on breast tissue type. The best results to detect MCs are achieved with the proposed approach in Fatty tissue (F) mammograms, according to the MIAS database. On the other hand, with Glandular (G) and Dense-Glandular (D) tissues, due to the tissue nature the detection becomes difficult. The approach reported in this work can be used as a basis to develop an automatic diagnostic system to aid the results on mammogram interpretation and to get an earlier and opportune diagnostic for breast cancer. The MCs detection stage could be improved to dense tissue and could be extended for other kind of lesions that are also breast cancer indications. After the detection stage, a segmentation stage could be implemented with fuzzy logic [2] or neural networks [7], [8]. Furthermore, to detect another kind of lesion, these could be classified into benign or malignant depending on shape and size characteristics.

REFERENCES

1. Akay, M (1997). Wavelet Applications in Medicine. *IEEE Spectrum*, **34** (5).
2. Cheng, H., Lui, YM, Feiimanis, RI (1998). A Novel Approach to Microcalcification Detection Using Fuzzy Logic Techniques. *IEEE Transactions on Medical Imaging*, **17** (6).
3. Zhao, D (1993). Rule-based Morphological Feature Extraction of Microcalcifications in Mammograms. *Proceedings of SPIE* 1905.
4. Strickland, R., Hahn (1996). Wavelet Transforms for Detecting Microcalcifications in Mammograms. *IEEE Transactions on Medical Imaging*, **12** (4).
5. Wang, T., Karayiannis, N (1998). Detection of Microcalcification in Digital mammograms Using Wavelets. *IEEE Transactions on Medical Imaging*, **17** (4).
6. Melloul, M., Joscowicz, L (2002). Segmentation of Microcalcification in X-ray Mammograms Using Entropy Thresholding. *In Proceedings of the 16th International Congress on Computer-Assisted Radiology and Surgery CARS/Springer*.
7. Gholamali, R., Jamarani, S (2005). Detecting Microcalcification Clusters in Digital Mammograms Using Combination of Wavelet and Neural Network. *In Proceedings of the Computer Graphics, Imaging and Vision: New Trends CGIV '05*.
8. Papadopoulos, A., Fotiadis, D.I., Likas, A (2005). Characterization of Clustered Microcalcifications in Digitized Mammograms Using Neural Networks and Support Vector Machines. *Artificial Intelligence in Medicine*.
9. Suckling J, Astley S, Betal D, Cerneaz N, Dance DR, Kok S-L, et al. (1994). The Mammographic Image Analysis Society Digital Mammogram Database. *International Congress Series 1069. Excerpta Medica* 375–378. Available at <http://peipa.essex.ac.uk/info/mias.html>
10. Burrus, CS., Gopinath, RA, Guo, H (1998). *Introduction to Wavelets and Wavelet Transforms*, Prentice Hall.
11. Gonzalez, RC, Woods, RE (2001). *Digital Image Processing*, Second Edition, Prentice Hall.
12. Lopez-Aligue, FJ, Poveda-Pierola, A., Acevedo-Sotoca, I., Garcia-Urra, F (2007). Detection of Microcalcifications in Digital Mammograms. *In Proceedings of the IEEE 29th Annual International Conference on Engineering in Medicine and Biology Society, EMBS 2007*. 3906–3909.
13. Shukla, PD (2003). *Complex Wavelet Transforms and Their Applications*. M.Phil. Thesis. University of Strathclyde. Scotland, UK.
14. Jamarani, SMH, Rezai-rad, G., Behnam, H (2005). A Novel Method for Breast Cancer Prognosis Using Wavelet Packet Based Neural Network. *In Proceedings of the IEEE 27th Annual International Conference on Engineering in Medicine and Biology Society, EMBS 2005*, 3414–3417.
15. Musoko, V (2005). *Biomedical Signal and Image Processing*. Ph.D. Thesis. Institute of Chemical Technology, Prague.
16. Alarcon-Aquino, V., Barria, JA (2009). Change Detection in Time Series Using The Maximal Overlap Discrete Wavelet Transform, *Latin American Applied Research: An International Journal*, **39** (2).
17. Selesnick, IW., Baraniuk, RG, and Kingsbury, NG (2005). The Dual-Tree Complex Wavelet Transform. *IEEE Signal Processing Magazine*, 123–151.
18. Mencattinni, A., Salmeri, M., Lojacano, R., Frigeno, M., et al. (2008). Mammographic Images Enhancement and Denoising for Breast Cancer Detection Using Dyadic Wavelet Processing. *IEEE Transactions on Instrumentation and Measurement*, **57** (7) 1422–1430.
19. Jansen M., Bultheel A (1999). *Asymptotic Behaviour of the Minimum Mean Squared Error Threshold for Noisy Wavelet Coefficients of Piecewise Smooth Signals*. Katholieke Universiteit Leuven. Department of Computer Science. Belgium.
20. Azzalini A., Farge M., Schneider K (2005). Nonlinear Wavelet Thresholding: A Recursive Method to Determine the Optimal Denoising Threshold. *Applied and Computational Harmonic Analysis*. Elsevier, **18**, 177–185.
21. Karahalios, A. H., Ioannis S. Boniatis, Spyros G. Skiadopoulos, Filipos N. Sakellaropoulos, et al. (2008). Breast Cancer Diagnosis: Analyzing Texture of Tissue Surrounding Microcalcification. *IEEE Transactions on Information Technology in Biomedicine*, **12** (6) 731–738.
22. Taswell, C (2000). The What, How and Why of Wavelet Shrinkage Denoising. *Computing in Science & Engineering*, **2** (3) 12–19.

